Interaction of CO_2 and CH_4 With Functionalized Periodic Mesoporous Phenylene–Silica: Periodic DFT Calculations and Gas Adsorption Measurements

Mirtha A. O. Lourenço,[a] Christophe Siquet,[b] Mariana Sardo,[c] Luís Mafra,[c] João Pires,[d] Miguel Jorge,[e] Moisés L. Pinto,[f] Paula Ferreira,[a] José R. B. Gomes[c*]*

[a]CICECO – Aveiro Institute of Materials, Department of Materials & Ceramics Engineering, University of Aveiro, 3810-193 Aveiro, Portugal

[b]LSRE, Faculty of Engineering, University of Porto, 4200-465 Porto, Portugal

[c]CICECO – Aveiro Institute of Materials, Department of Chemistry, University of Aveiro, 3810-193 Aveiro, Portugal

[d]CCB – Center of Chemistry and Biochemistry, Faculty of Sciences, University of Lisbon, 1749-016 Lisboa, Portugal

[e]Department of Chemical and Process Engineering, University of Strathclyde, 75 Montrose Street, Glasgow G1 1XJ, United Kingdom

[f]CERENA, Instituto Superior Técnico, University of Lisbon, Av. Rovisco Pais, n° 1, 1049-001 Lisboa, Portugal

ABSTRACT

Non-functionalized and functionalized periodic mesoporous phenylene-silicas (Ph-PMOs) with different kinds of amine groups were prepared and their capacity to uptake CO_2 and CH_4 molecules were experimentally evaluated considering biogas upgrading. It was found that aminopropyl groups grafted to the free silanols of the Ph-PMO displayed the highest selectivity for CO_2 gas, adsorbing 26.1 times more CO_2 than CH_4 at 25 °C. The interaction effect of the surface of these materials with the CO_2 or CH_4 molecules was obtained through the calculation of the Henry constants, and the adsorption mechanisms involved were elucidated from density functional theory calculations. The good synergy between experimental gas adsorption and computational studies suggests that the latter can be used to guide the experimental synthesis of more effective materials. Thus, our computational studies were extended to PMOs with other functional groups having different polarity for predicting interaction energies with CO_2 and thus identifying the most promising candidates for experimental synthesis.

KEYWORDS: CO_2 Adsorption, Periodic Mesoporous Organosilica; Gas separation; Periodic Models; Density Functional Theory.

1. INTRODUCTION

The growth of the world population, the increasing environmental concerns and the rising oil prices lead to a high demand for energy. In this respect, biogas, a mixture of gases rich in methane (CH_4) resulting from anaerobic decomposition of organic matter, can be an excellent source for obtaining clean, natural, and renewable alternative energy.[1] However, the presence in large amounts of the carbon dioxide (CO_2) contaminant (approx. 20-50%) requires biogas upgrading[2,3] to obtain pure CH_4 streams. Therefore, strong efforts are being made to develop materials for the separation of these gases.[4] Conventional adsorbents with different composition and structure such as activated carbons,[5] zeolites,[6] clays,[7] biosorbents,[8] polymeric adsorbents,[9] polymeric/inorganic hybrids[10] and silica-based mesoporous materials[11] have been proposed but showed low separation performances. Thus, there is a strong need for a major breakthrough in finding an optimal adsorbent for this purpose, which should maximize the following features: high capacity, good selectivity, long-term durability, fast uptake, reasonable low cost, easy regeneration consistent with negligible capacity loss on multiple adsorption/desorption cycles, and low toxicity[12].

Herewith, we assess the use of functional periodic mesoporous phenylene-silicas (Ph-PMOs) as adsorbents for CO_2/CH_4 gas separation due to the intrinsic characteristics of this kind of materials – high specific surface areas, high pore volumes and high thermal stability.[13–15] These hybrid materials have also a narrow distribution of the meso- and molecular-scale periodicities allowing efficient diffusion of the molecules into the channels. Furthermore, chemical modification of the framework benzene moieties with, for instance, amino basic groups, can be accomplished to optimize their features for the separation of CO_2/CH_4, i.e., by enhancing interactions with one of the gases. These functional groups can additionally

display interesting synergistic effects in materials that already exhibit high π-π conjugation and mixed hydrophobic/hydrophilic character.

Our main aim in this work is to introduce amine modifications in Ph-PMO in order to increment the interactions with CO_2 without improving those with CH_4 gases. This strategy will improve the potential of these materials to separate CO_2/CH_4 mixtures, i.e., making these materials candidates for biogas upgrading. Recently, we described and understood the amination of the Ph-PMO (NH_2-Ph-PMO) with different pore sizes (2.4 – 3.7 nm) and tested their performance on the CO_2 and CH_4 adsorption.[16] We observed that the CO_2 affinity on these materials can be directly correlated to the amount of T^2 free silanols and the amination on the phenylene moieties is only effective on materials with small pore size, improving the affinity to the CO_2 gas. In the present work, non-functionalized (Ph-PMO) and amine functionalized Ph-PMOs (NH_2-Ph-PMO), having pore sizes of approximately 2.5 nm, were synthesized according to previously reported procedures.[17,18] Two additional materials, i.e., APTMS@Ph-PMO and APTMS@NH_2-Ph-PMO, were obtained by post-grafting 3-aminopropyltriethoxysilane (APTMS) to the Ph-PMO and NH_2-Ph-PMO. Thus, different kinds of amines were incorporated into the Ph-PMO through different methodologies. Theoretical and experimental gas adsorption studies were carried out to evaluate the affinities of these materials towards CO_2 and CH_4, and to understand the interactions between the materials' functional groups and these two gases. To the best of our knowledge only a single previous experimental study describes the grafting of the APTMS to the free silanols of the Ph-PMO, but the resulting material (APTMS@Ph-PMO) presented large pore sizes and was only tested on the CO_2 adsorption.[19] Similarly, only a few theoretical studies of PMOs exist,[20] and none of them evaluate phenylene bridge or silanol functionalized PMO materials for gas

adsorption/separation. After validation of the computational approach, additional calculations were performed to predict if other functional groups, e.g. $–NO_2$, $–SO_3H$, $–NH(^iPr)$ and $–CH_2NH_2$, were also effective in promoting selective interactions with CO_2. The results of our study highlight the potential of a synergistic approach involving theory and experiment to guide the rational design of materials for gas separation applications.

2. EXPERIMENTAL AND COMPUTATIONAL DETAILS

2.1. Synthesis of PMOs. The Ph-PMO was synthesized following a method previously described in the literature.[21,22] The 1,4-bis(triethoxysilyl)benzene (BTEB) precursor[23] was hydrolyzed and condensed around a supramolecular structure directing agent, the dodecyltrimethylammonium bromide template (C_{12}TMA, Aldrich, 98%). The template extraction was achieved with an ethanol–HCl solution. The incorporation of functional amino groups into the phenylene rings (to yield the NH_2-Ph-PMO material) was achieved upon treatment with very strong acid solutions of HNO_3–H_2SO_4 and $SnCl_2$–HCl (scheme 1) using the procedure described by Inagaki *et al*.[17] The Ph-PMO and the NH_2-Ph-PMO (1 g) were dried at 80 ◦C under vacuum atmosphere during 3 h.

The materials APTMS@Ph-PMO and APTMS@NH_2-Ph-PMO were obtained from Ph-PMO and NH_2-Ph-PMO, respectively. After the activation of the pores, dry dichloromethane (10 mL) was added and (3-aminopropyl)trimethoxysilane (0.439 g) was added drop wise to the suspension. The mixtures were vigorously stirred for 48 h. The obtained materials were filtered off and further washed with a large amount of distilled water and dried in an oven at 60 °C overnight. The APTMS post-grafting reaction was repeated for two additional cycles.

2.2. Characterization of PMOs. The structural order and the textural physical properties of all PMO materials were evaluated by powder X-ray diffraction (PXRD), -196 °C N_2-sorption isotherms and Transmission Electron Microscopy (TEM). ^{29}Si Magic-Angle Spinning (MAS) Nuclear Magnetic Resonance (NMR) and ^{13}C and ^{29}Si Cross-Polarization (CP) MAS NMR spectra were collected to check the stability of the Si-C bonds in the PMOs and to verify the chemical structure of the organic bridge, respectively. Fourier Transform Infrared (FTIR) spectroscopy was also used to verify the chemical bonds of all prepared PMOs. The nitrogen density was determined by Elemental Analysis (EA). More information concerning the measurements is available in Supporting Information (SI).

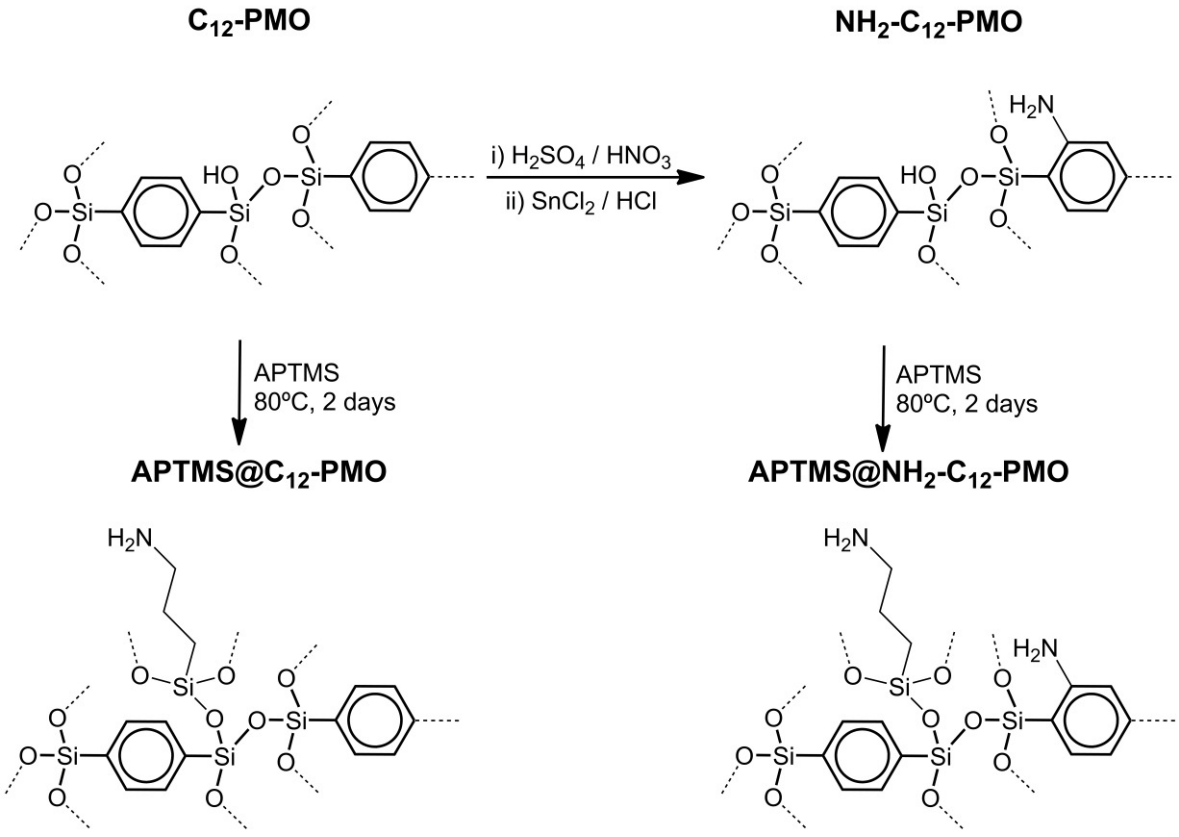

Scheme 1. Functionalization of Ph-PMO material with amine groups.

2.3. Gas adsorption details. Adsorption isotherms of CO_2 and CH_4 on prepared samples were measured up to 1000 kPa at 25 °C, using the volumetric method. These experiments were carried out on a custom-made stainless steel volumetric apparatus, with a pressure transducer (Pfeiffer Vacuum, APR 266), and equipped with a vacuum system that allows a vacuum better than 10^{-2} Pa. The temperature was controlled with a stirred thermostatic water bath (Grant Instrument, GD-120) and before every experiment the samples were degassed for 2.5 h at 150 °C. Each experimental pure component adsorption isotherm was fitted using the Virial model, where the non-ideality of the gas phase was taken into account by using the second and third virial coefficients, and the experimental excess adsorbed amounts were converted to the absolute adsorbed amounts by taking into account the porous volume of the material and the density of the gas phase using the virial coefficients. Selectivity values were estimated using a method proposed by Myers[24] and the implementation is described in detail in previous works.[25] The virial equation of state fitted to the adsorption data is in the form:

$$p = \frac{n^{ads}}{K}\exp\left(C_1 n^{ads} + C_2 n^{ads^2} + C_3 n^{ads^3}\right) \quad (1)$$

where K is the Henry constant, and C_1, C_2, and C_3 are the constants of the virial-series expansion.

Adsorption isotherms of pure CO_2 and CH_4 were also measured on as-synthesized and amine-modified PMO materials at 35 °C and pressures up to 200 kPa using an in-house built manometric apparatus. The samples were activated first at 80 °C during 5 h and then at 160 °C during 10 h, under vacuum of ca. 1.4 kPa. The CO_2 and CH_4 gases were used as provided

by Air Liquide (France), with a purity of 99.998% and 99.95 %, respectively. The experimental adsorption measurements technique adopted was also previously described.[26]

2.4. DFT Calculations. Periodic slab calculations were performed with the VASP computer code.[27–29] Density functional theory (DFT) calculations considered the Perdew-Burke-Ernzerhof (PBE) exchange-correlation functional,[30] based on the generalized-gradient approximation (GGA). The non-spin polarized DFT calculations include a correction for the van der Waals interactions according to the D2 method proposed by Grimme using the default parameters.[31–33] The suitability of the PBE-D2 approach is supported by results in a previous study where the calculated interaction energy for CO with Ph-PMO (-14.3 $kJ \cdot mol^{-1}$)[34] was found to be in close agreement with the experimental interaction enthalpy (-13.2 $kJ \cdot mol^{-1}$)[35] obtained from variable temperature infrared (VTIR) spectroscopy and with the range of binding energies calculated with the B3LYP-D approach for CO interacting with cluster models.[20,35] Valence electrons were described by plane-wave basis sets and core electrons with projector-augmented wave (PAW) potentials.[36] A kinetic energy cutoff of 415 eV was used. The atomic positions in the supercells used to model the walls of the different PMO materials were fully relaxed with the quasi-Newton algorithm, and the stopping-criteria for electronic and ionic updates were 10^{-7} eV and -0.05 eV/Å, respectively. Dipole corrections in the direction perpendicular to the PMO wall were applied.

The cell dimensions and the atomic coordinates for the structural model of the walls in the Ph-PMO material were taken from a previous work by Martínez and Pacchioni.[34] The structure is shown in Figure 1 and corresponds to a sequence of six and four member rings of organosilica tetrahedra with T^3 to T^2 [T^n=$RSi(OH)_{(3-n)}(OSi)_n$, in which R represents an organic group] silicon environments in a ratio of 2:1, grounded on information from solid

state NMR obtained by Comotti et al.[37] Notice that Martínez and Pacchioni[34] considered also a structural model of the walls of the nanopores based on a sequence of six member rings only, with T^3 to T^2 in a ratio of 1:1, derived from the three-dimensional periodic lattice having the planes of the aromatic rings parallel to each other reported by Inagaki et al.[21], but found the former structure, with non-planar benzene moieties, to be more stable (~ 30 $kJ \cdot mol^{-1}$ per formula unit) than the latter. Important for the discussion below is the fact that the interaction energy of CO_2 – either in the model with six and four member rings or with six rings only – is about 50% larger than that corresponding to CH_4. Thus, the information obtained with one or the other model is expected to be qualitatively similar.

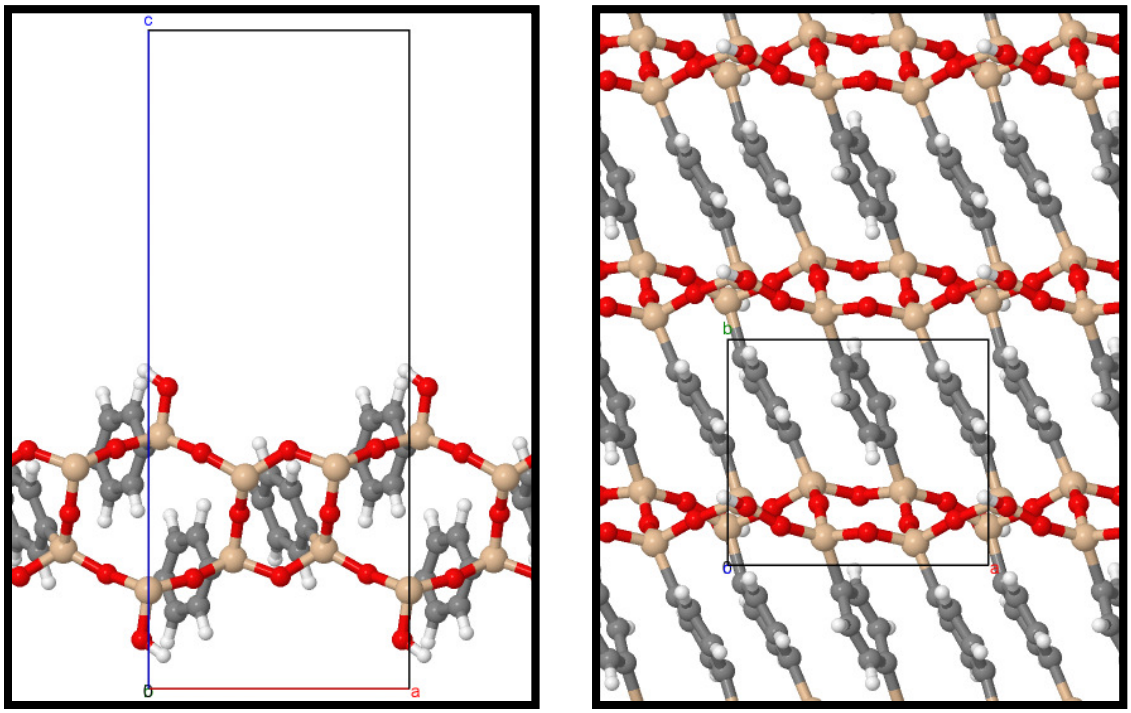

Figure 1. Side (left) and top (right) views of the unit cell (inline) used to model the Ph-PMO material with fully-optimized atomic positions. Color code for atomic spheres is: H, white; C, grey; O, red; and Si, pink.

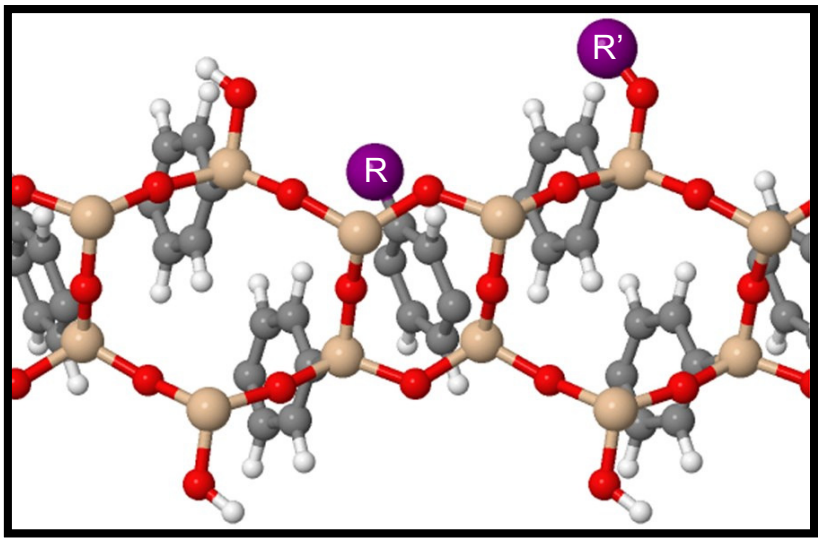

Figure 2. Functionalization of the Ph-PMO by post-modification, i.e., by replacement of a single H atom in the aromatic rings with an **R** group (R = NH_2, NO_2, NH-*i*-Pr, CH_2NH_2 and SO_3H) and by grafting, i.e., by substitution of a silanol H atom by an **R'** group (R' = APTMS). Purple is used for the substituent groups and color code for remaining spheres as in Figure 1.

The structures of the functionalized materials were obtained by single substitution of protons in the aromatic rings of the unit cell of Ph-PMO shown in Figure 1 by different functional **R** groups, e.g. $–NH_2$, $–NO_2$, –NH-*i*-Pr, $–CH_2NH_2$ and $–SO_3H$ (cf. Figure 2). The selection of the functional groups considered above was primarily based on their different polarities and on the presence of amine moieties, which in principle will be beneficial for improving the interactions with CO_2 without changing significantly those with CH_4. The substitution was made at several different positions and the structures of the models obtained were fully relaxed. Since the unit cell in Figure 1 contains three phenyl groups, this strategy led to the functionalization of 33% of the aromatic rings, which is similar to the maximum functionalization obtained experimentally (see below). The model corresponding to the functionalization with the APTMS group (**R'**) was obtained by introduction of this group at

the free silanol (substitution of the proton by APTMS) available in the structure of the Ph-PMO model (cf. Figure 2). The percentage of APTMS groups grafted to the PMO was 50%. The models described above were used to study separately the adsorption of CO_2 and CH_4 by fully optimizing the atomic positions of the adsorbate/adsorbent complex. The interaction energies were calculated as standard practice by subtracting the energies of the individual adsorbate and adsorbent fragments from the energy of the complex. Thus, negative values of the energy correspond to favorable gas/PMO interactions.

3. RESULTS AND DISCUSSION

3.1. Characterization of Materials. The structural integrity of the prepared adsorbents was determined from the combination of PXRD and N_2 sorption isotherms. Figure S1 (SI) shows the PXRD diffraction patterns of Ph-PMO, NH_2-Ph-PMO, APTMS@Ph-PMO and APTMS@NH_2-Ph-PMO materials. The pristine Ph-PMO possesses a two-dimensional hexagonal symmetry (*p6mm*) lattice with a *d* spacing of 3.59 nm for the strong (100) reflection at low-angle (Table S1, SI). In the case of the aminated samples, slight changes are observed in the PXRD (Figure S1, SI) corresponding to the loss of definition of the 2D hexagonal arrangement, which is in agreement with the introduction of the amine functional groups inside the pores since some loss of regularity in the structure is expected during the amination reactions.[15] The lattice parameters of the hexagonal array of mesopores (calculated from the 2θ values of the (100) peaks) obtained for the NH_2-Ph-PMO, APTMS@Ph-PMO and APTMS@NH_2-Ph-PMO samples are 3.63, 3.34 and 3.50 nm, respectively (Table S1, SI). The molecular-scale periodicity in the Ph-PMO pore walls along the channel direction is observed by the presence of a medium-range reflection at $d \sim 0.76$ nm.[21] The pristine material and all amine functionalized materials present these peaks at the same *d* spacing.

Thus, the preparation of different amine functionalized phenylene PMOs is made with the preservation of both meso- and molecular-order.

The presence of different amine functional groups inside the pore was confirmed by N_2 adsorption–desorption experiments, with isotherms depicted in Figure S2 (SI). The parent Ph-PMO exhibits a type IV isotherm[38], typically detected for conventional mesoporous materials such as MCM-41[39], indicating narrow distribution of mesopores of uniform size. The introduction of the amine functional groups (NH_2 group in the aromatic moieties or/and APTMS covalently bonded to the free silanols) into the mesochannels is supported by the reduction of the BET surface area and pore volume (Table S1 and Figure S2, SI). The Ph-PMO, NH_2-Ph-PMO, APTMS@Ph-PMO and APTMS@NH_2-Ph-PMO materials present BET surface areas of 1004, 924, 634 and 305 $m^2 \cdot g^{-1}$, respectively (Table S1, SI). The reduction in surface area and pore volume is much more pronounced for the APTMS-containing materials, due to the bulky nature of this group, which protrudes within the pore space. A comparison of the pore size distribution (PSD) curves of pristine PMO and amine functionalized Ph-PMO materials is presented in Figure S3 (SI) and in Table S1, and reveals a maximum shifting from 2.54 to 2.23 nm, respectively.

Solid-state ^{13}C CP-MAS NMR, ^{29}Si MAS and CP-MAS NMR spectra of Ph-PMO, NH_2-Ph-PMO, APTMS@Ph-PMO and APTMS@NH_2-Ph-PMO materials are displayed in Figures 3 and S4 (SI), respectively. ^{13}C CP-MAS NMR spectra support the different amine functionalizations of Ph-PMO materials. The parent PMO (Figure 3a) shows a characteristic resonance at 133 ppm that corresponds to the C of the phenylene bridge as reported in the literature.[21] On the other hand, the spectra for the NH_2-Ph-PMO material presents resonances at *ca*. 121, 133 and 151 ppm assigned to the distinct sp^2 carbons associated to the amine

functionalized phenylene group. These results are in agreement with previous reports for NH_2-Ph-PMO.[17] As expected, the spectrum for APTMS@NH_2-Ph-PMO also displays the three characteristic peaks corresponding to aminated phenyl groups, while that of APTMS@Ph-PMO displays the single resonance at 133 ppm. The grafting of the APTMS to the free silanols in both Ph-PMO and NH_2-Ph-PMO is verified by ^{29}Si NMR measurements (Figure S4, SI). The three resonances appearing at *ca.* 10, 22 and 43 ppm in the ^{13}C CP-MAS NMR spectra correspond to the carbons of the propyl chain of the APTMS@Ph-PMO and APTMS@NH_2-Ph-PMO materials (Figure 3 c-d). Figure 3d shows a tiny peak at around 164 ppm that is assigned to amines binding CO_2 from the atmosphere.

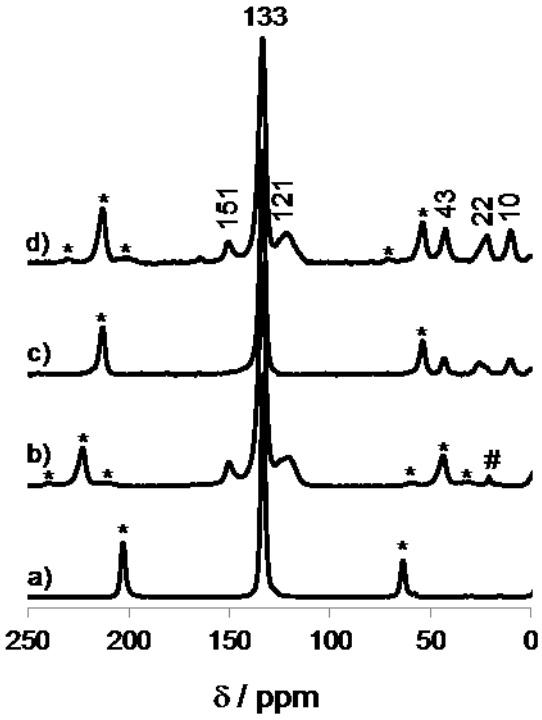

Figure 3. ^{13}C CP-MAS NMR spectra of a) Ph-PMO, b) NH_2-PMO, c) APTMS@Ph-PMO and d) APTMS@NH_2-Ph-PMO. The asterisks correspond to the spinning side bands. The number symbol denotes traces of surfactant.

The ^{29}Si MAS and CP-MAS NMR spectra (Figure S4, SI) of the pristine Ph-PMO display resonances at *ca.* -82, -71 and -61 ppm assigned to T^3, T^2 and T^1 (T^m = $SiR(OSi)_m(OH)_{3-m}$) organosiliceous species, respectively. The strong acid treatment used in the amination reaction of the pristine Ph-PMO material induces, in very slight amounts, the carbon–silicon bond cleavage of the BTEB precursor; this is observed by the presence of a faint resonance at *ca.* -91 ppm (Figure S4, SI) corresponding to Q^2 [Q^n = $Si(OSi)_n(OH)_{4-n}$] species. The grafting of the APTMS to the T^1 and T^2 silanols of both Ph-PMO and NH_2-Ph-PMO leads to the reduction in intensity of the resonances corresponding to these species (see Figure S4 and Table S2, SI) with respect to T^3 environments. In addition, a new resonance appears at *ca.* -58 ppm, labeled as $T^{2'}$ in this work (Figure S4, SI), corresponding to the silanol species of the APTMS silicon atom. It is worth mentioning that the difference between T^2 and $T^{2'}$ species is due, respectively, to the presence of an aromatic and an alkylamine carbon residue bonded to the Si center.

The functionalization of the Ph-PMO material was also followed by FTIR (Figure S5, SI). The presence of aromatic primary amines in the NH_2-Ph-PMO is confirmed by the C–N stretching band at 1265 cm^{-1} and the in plane N–H bending vibration close to 1620 cm^{-1}. This latter band overlaps with the band of H–O–H bending vibrations and the N–H stretching modes appearing at 3400 and 3352 cm^{-1}. The amine group of the APTMS in APTMS@Ph-PMO and in APTMS@NH_2-Ph-PMO materials presents N–H stretching modes appearing at 3356 $cm^{-1}$and at 3354 and 3402 cm^{-1}, respectively. The aromatic C–H stretching bands appear in the parent PMO at 3065 cm^{-1}, while in the NH_2-Ph-PMO they appear at 3066 cm^{-1} and in the APTMS grafted amine functionalized and non-functionalized Ph-PMOs they appear at 3064 cm^{-1}. The APTMS@Ph-PMO and the

APTMS@NH_2-Ph-PMO materials present the C–H stretching vibrations for saturated aliphatic species at 2862 and 2928 cm^{-1} and at 2867 and 2939 cm^{-1}, respectively.

The introduction of the amine group in the phenylene moieties of Ph-PMOs and the grafting of APTMS to the free silanols of Ph-PMO lead to a reduction of thermal stability from 600 ºC to 400 ºC and to 300 ºC, respectively, as observed by TGA (Figure S6, SI). The Ph-PMO material presenting both types of amines (NH_2 and APTMS) is thermally stable only up to 250 ºC.

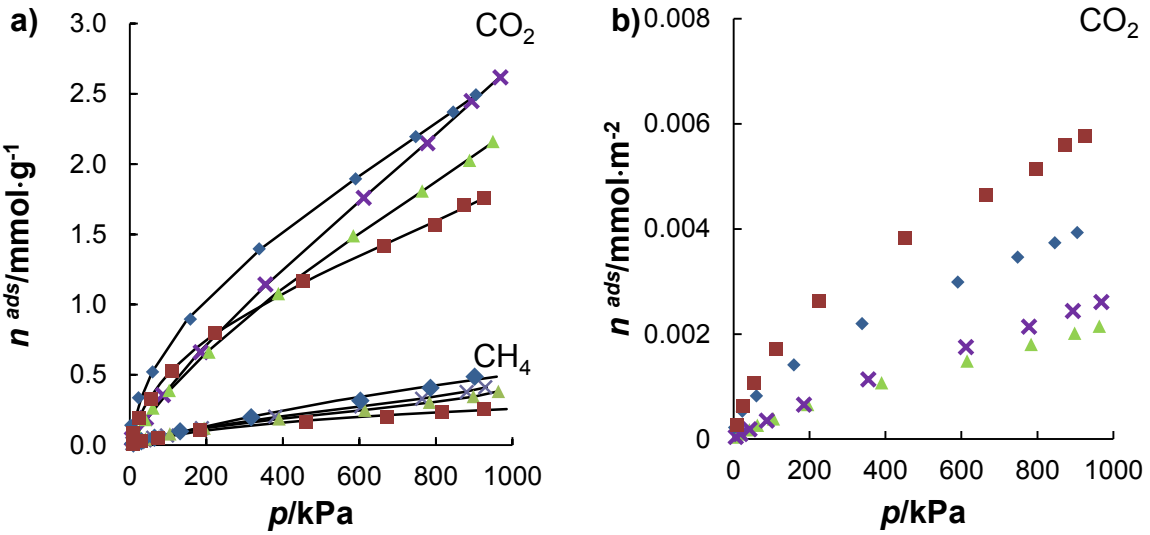

Figure 4. Adsorption equilibrium isotherms of CO_2 and CH_4 at 25 °C on the prepared materials expressed as a) mmol·g^{-1} and b) mmol·m^{-2}. Solid lines were obtained by fitting the experimental points to the Virial model. ▲ labels correspond to Ph-PMO, × labels correspond to NH_2-Ph-PMO, ♦ labels correspond to APTMS@Ph-PMO, and ■ labels correspond to APTMS@NH_2-Ph-PMO.

Table S3 (SI) presents the density of amine groups in the Ph-PMO materials determined by EA. The NH_2-Ph-PMO has a nitrogen percentage of 2.58% that corresponds to amine density of 1.85 mmol·g^{-1}. The grafting of APTMS into the Ph-PMO leads to a density of amine groups of 1.39 mmol·g^{-1}. The APTMS@NH_2-Ph-PMO has a total amine density of 2.60 mmol·g^{-1}, which results from the sum of the aromatic amine density of 1.85 mmol·g^{-1} and of the APTMS amine density of 0.75 mmol·g^{-1}.

3.2. Experimental pure-component adsorption isotherms. Pure-component adsorption isotherms of CO_2 and CH_4 at 25 °C are shown in Figure 4. The Henry's constant (K) was determined for each pure gas adsorbed in each material using the Virial model in order to evaluate the interaction of the chemical surface of our materials with pure CO_2 and pure CH_4 at low coverage. The fitting parameters for the Virial model are provided in Table 1.

The adsorption isotherms in Figure 4 suggest that the introduction of the amines into the Ph-PMO material leads to an increase in the amount of adsorbed CO_2 and in the Henry's constants, increasing in the order Ph-PMO < NH_2-Ph-PMO < APTMS@NH_2-Ph-PMO < APTMS@Ph-PMO, i.e., the non-functionalized material presents less affinity for CO_2 than the aminated samples. In the case of methane adsorption, the Ph-PMO material has the highest adsorption affinity, manifested in the highest Henry's constant (Table 1), although the differences observed for the different materials suggest that in all cases the adsorption is significantly lower than that observed for CO_2. The amine functionalization of the aromatic moieties of the Ph-PMO leads to, as expected, a reduction of the BET surface area and pore volume (Table S1, SI) but the CO_2 adsorption affinity is slightly increased (Table 1). This is a consequence of the introduction of amine groups covalently bonded to the phenylene

bridges of the Ph-PMO material, corresponding to a nitrogen content of 2.58 % (Table S3, SI). This is better noticed when the adsorption isotherms are normalized by the BET surface area (Figure 4b). Therefore, the introduction of an aromatic amine into the PMO channels reveals that the chemical functionalization of the PMO material is more important for CO_2 capture than the amplitude of textural properties such as the surface area and pore diameter. This is a consequence of the energetically more important interactions between the CO_2 molecules and the amine groups than with other sites available in the parent Ph-PMO material.

Table 1 demonstrates that the NH_2-Ph-PMO material has slightly lower affinity for CH_4 than Ph-PMO, suggesting that the introduction of the amine moiety at the aromatic rings weakens the interaction of PMO with CH_4. This tiny reduction in the CH_4 adsorption is also in accordance with the decrease in the BET surface area and pore volume. Still, the adsorption of CH_4 is small in both cases.

Table 1. Virial coefficients (C_1 and C_2) and Henry's constants (K) for the adsorption of methane and carbon dioxide at 25 °C on the prepared materials.[a]

Gas	Material	K (mmol g^{-1} kPa^{-1}) x 10^{-2}	C_1 g $mmol^{-1}$	C_2 (g $mmol^{-1}$)^2	C_3 (g $mmol^{-1}$)^3	*Selectivity*
CH_4	Ph-PMO	0.13	7.458	-11.487		
	NH_2-Ph-PMO	0.11	5.200	-7.296		
	APTMS@Ph-PMO	0.07	0.797			
	APTMS@NH_2-Ph-PMO	0.08	4.504			
CO_2	Ph-PMO	0.45	0.562	-0.112		3.2 (3.5[b])
	NH_2-Ph-PMO	0.48	0.507	-0.151	0.015	3.6 (4.4[b])
	APTMS@Ph-PMO	1.83	1.647	-0.476	0.048	6.7 (26.1[b])
	APTMS@NH_2-Ph-PMO	1.08	1.750	-0.434		6.2 (13.5[b])

[a] Obtained by nonlinear least-squares fitting of the virial equation to the adsorption data. [b]Ratio of the Henry's constant for CO_2 to that for CH_4.

The grafting of the APTMS onto the silanols of the pristine Ph-PMO to obtain the APTMS@Ph-PMO material is accompanied by a very pronounced decrease of its surface area and pore volume. The nitrogen content (Table S3, SI) of APTMS@Ph-PMO is 1.93 %, which can be compared with that determined for NH_2-Ph-PMO (2.58 %). Interestingly, the former displays higher adsorption capacity and Henry's constant for CO_2 than the latter material, thus revealing that the type of amine has a stronger influence on the sorption capacity for CO_2 than the amount of nitrogen introduced in the PMO channels, suggesting that alkyl amines interact more favorably with CO_2 than the aromatic amines, because the former amines present higher basicity than the latter.[40]

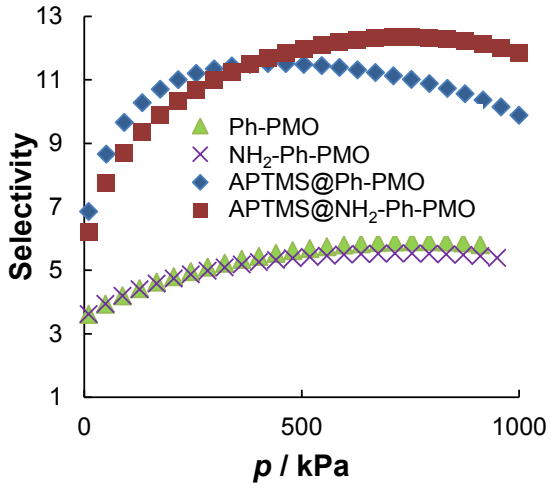

Figure 5. Average selectivity for the CO_2/CH_4 separation on the different materials at 25 °C. ▲ labels correspond to Ph-PMO, × labels correspond to NH_2-Ph-PMO, ♦ labels correspond to APTMS@Ph-PMO, and ■ labels correspond to APTMS@NH_2-Ph-PMO.

The APTMS@NH_2-Ph-PMO material shows lower adsorption capacity for CO_2 (cf. Figure 4a) than APTMS@Ph-PMO, but when the adsorption isotherm is expressed taking into

account the BET surface area (Figure 4b) a substantial increase in the adsorption of CO_2 can be perceived. This is likely to be due to the larger degree of amination resulting from the simultaneous presence of aromatic and alkyl amines in the same PMO material, despite the concomitant lower BET surface area (305 $m^2 \cdot g^{-1}$) and pore size (2.23 nm) when compared with the other materials described above, cf. Table S1 (SI). Note that this material only presents 0.75 $mmol \cdot g^{-1}$ of APTMS amine density, much lower than in APTMS@Ph-PMO (1.39 $mmol \cdot g^{-1}$), and this type of amine interacts more strongly with the CO_2 molecule than the aromatic amine.

The Ideal Adsorbed Solution Theory[41] was applied to the analysis of the adsorption data by fitting the Virial equation to the pure-component isotherms and calculating the selectivity of the separation and the equilibrium phase diagrams using a method proposed by Myers[24] with the implementation described in detail in previous works.[25,42] As can be seen in Figure 5, the differences in the predicted selectivities exhibited by the different materials for the CO_2/CH_4 separation can be quite large. In fact, the materials with APTMS groups grafted to the silanols of the PMO present much higher selectivity values than Ph-PMO and NH_2-Ph-PMO. These two latter materials present similar selectivity, but we can notice a slight increase in the selectivity at low pressures for NH_2-Ph-PMO (3.6 at 10 kPa) when compared with Ph-PMO (3.2 at 10 kPa). This indicates that the aromatic amine is not bringing the desired effect in the selectivity over the entire range of pressures (Table 1). Variation of selectivity with pressure is also seen in the case of the APTMS materials. At low pressures, APTMS@Ph-PMO presents higher selectivity than APTMS@NH_2-Ph-PMO but this ordering is reversed at higher pressures. This is most probably related with the kind of amines and their amount present on the materials. The APTMS@Ph-PMO material presents only alkyl amines that

seem to interact more strongly with CO_2 than aromatic amines. Alkyl amines are also available in APTMS@NH_2-Ph-PMO material but their amount, determined by EA, is one half of the amount of aminopropyl groups presented in APTMS@Ph-PMO (Table S3, SI). Thus, at low pressure, APTMS@Ph-PMO shows better selectivity than APTMS@NH_2-Ph-PMO because of the more important role of the type of amine than of its quantity. Still, the nitrogen content in the latter PMO is larger than that in the former (2.60 versus 1.39 $mmol \cdot g^{-1}$). The interaction of CO_2 with the aromatic amines is less favorable than with the alkylamines of grafted APTMS moieties but is more stable than any other site available in these PMOs. Hence, at high pressure, the larger amount of amines in APTMS@NH_2-Ph-PMO dictates a better selectivity for CO_2.

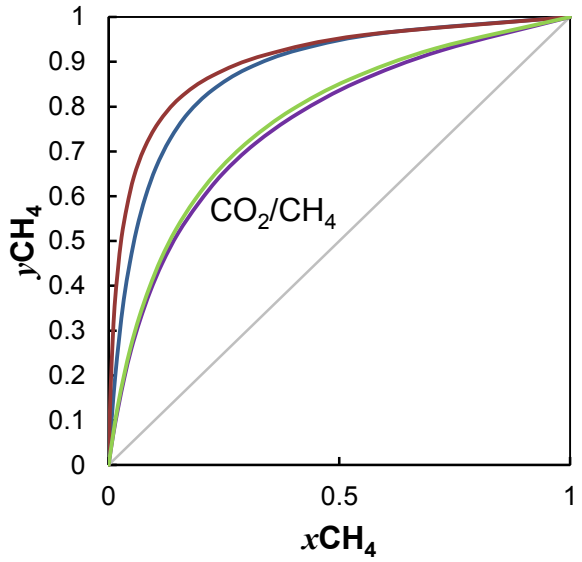

Figure 6. Isothermal (25 °C), isobaric (500 kPa) *xy* phase diagrams of the CO_2/CH_4 mixtures on, from top to bottom, APTMS@NH_2-Ph-PMO (brown line), APTMS@Ph-PMO (blue line), Ph-PMO (green line) and NH_2-Ph-PMO (purple line). y_{CH_4} is the molar fraction of methane in the gas phase; x_{CH_4} is the molar fraction of methane in the adsorbed phase.

These effects are even clearer in the ratio of the values of the Henry constants determined for CO_2 and CH_4 adsorption on each of the materials studied experimentally in this work (Table 1), which can be also used as an estimate of the ability of the materials for separating these gases. As can be seen in Table 1, the largest ratio was calculated for APTMS@Ph-PMO, which appears to be the most interesting adsorbent for CO_2/CH_4 separation.

The impact of all of the variables on the separation is illustrated in Figure 6, where it can be observed that APTMS@NH_2-Ph-PMO shows slightly better performance than APTMS@Ph-PMO. Moreover, these two materials are much better than Ph-PMO and NH_2-Ph-PMO. Considering a 0.5 molar composition of methane (y_{CH_4}), a reasonable value for biogas composition and some natural gas sources, the composition in the adsorbed phase (x_{CH_4}) is 0.02 on APTMS@NH_2-Ph-PMO and 0.06 on APTMS@Ph-PMO, at 500 kPa and 25 °C. Thus, the adsorbed phase is much richer in carbon dioxide than in methane for both materials with an adsorption of almost pure carbon dioxide (about 0.94 – 0.98 molar composition at 500 kPa and 25 °C) at 0.5 composition in the gas phase. Complete phase diagrams were also obtained (Figure S7, SI), which confirm a similar performance of these two materials.

Important for establishing the adequacy of these materials for typical adsorptive applications is the understanding of any structural changes upon degasification. After adsorption experiments, the aminated materials were reactivated using vacuum during 4 h at 100 °C.

The ^{15}N CP-MAS NMR spectrum of reactivated NH_2-Ph-PMO (Figure 7a) presents a peak corresponding to an aromatic amine at *ca.* -321 ppm, which is in agreement with the literature.[17] The absence of additional peaks in NH_2-Ph-PMO confirms that no CO_2

molecules are left covalently bonded to the aromatic amines of the material. Upon grafting with APTMS (APTMS@NH_2-Ph-PMO), four peaks were observed at *ca.* -262, -295, -320, and -348 ppm (Figure 7b). The latter two resonances are assigned to the aromatic amine and to the propylamine groups, respectively. The remaining resonances at *ca*. -262 and -295 ppm are assigned to species containing a carbonyl group resulting from the chemisorption of the CO_2 molecules. The presence of such species is also evident in the ^{13}C CP-MAS NMR showing resonances at *ca.* 178 and 164 ppm (Figure S8, SI), confirming the observations in the ^{15}N CP-MAS spectra, *i.e.*, a minor quantity of CO_2 remains bonded to the amines after activation at 100 °C. The ^{13}C resonance appearing at 164 ppm has been assigned to carbamate species by solid-state NMR and FTIR,[43] and is associated to the presence of the peak at -265 ppm in the ^{15}N CP-MAS NMR. The peak at 178 ppm appears only when CO_2 is adsorbed into the APTMS@NH_2-Ph-PMO material, which coincides with the presence of a distinct resonance at -262 ppm in the ^{15}N CP-MAS NMR for this same material. Thus, it is assumed that this resonance, in a chemical shift region typical of carbonyl groups, is due to a chemisorbed CO_2 species involving the simultaneous participation of the aromatic and aliphatic amines. The nature of such species cannot be unambiguously assigned from the data in the present study as this would require further experiments under well controlled conditions (pressure, temperature, moisture levels).

The spectrum of APTMS@Ph-PMO after material activation shows the presence of two peaks at *ca.* -293 and -352 ppm (Figure 7c). The latter peak is assigned to APTMS attached to the surface of the material, while the former peak corresponds to carbamate species as observed for analogous materials also functionalized with the aminopropyl group.[43] The persistence of CO_2 species after the degassing procedure above-mentioned is not surprising.

Indeed, it was previously shown that higher temperature was needed (about 150 ºC) to completely remove the CO_2 from amine functionalized materials, and at 100 °C only about 91% of bonded CO_2 could be removed.[43]

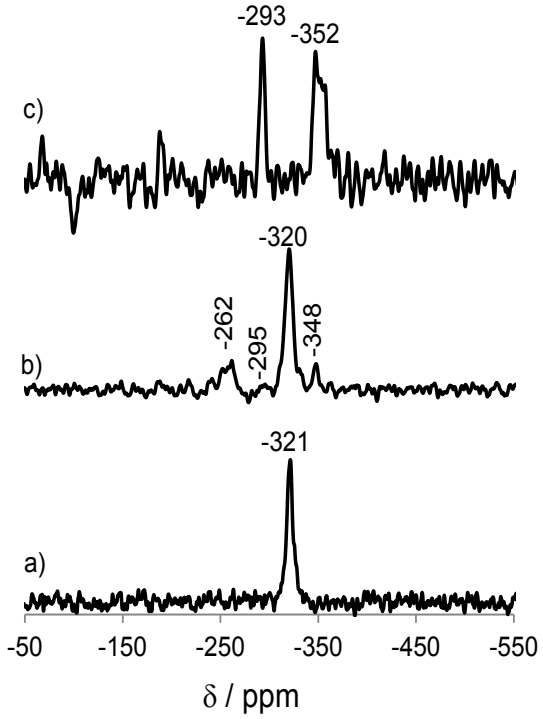

Figure 7. ^{15}N CP-MAS NMR spectra of the reactivated materials: a) NH_2-Ph-PMO; b) APTMS@NH_2-Ph-PMO; and c) APTMS@Ph-PMO after a first cycle of CO_2 adsorption.

All prepared materials were also tested for adsorption of pure CH_4 and CO_2, but measured in a pressure range between 0 and 200 kPa at 35 °C. Figure S9 and Table S4 (SI) show the results obtained for the most promising material, APTMS@Ph-PMO. As expected, APTMS@Ph-PMO adsorbs more CO_2 amount at 25 °C than at 35 °C, given that adsorption is an exothermic process. The CH_4 pure adsorption capacities and the related Henry's

constant are similar for both temperatures (25 °C and 35 °C), but this is most likely because of the low adsorbed amounts of this gas together with the relatively small temperature difference between isotherms (10 ºC), which makes it difficult observe the effect of temperature.

3.3. Computer simulations of all prepared functionalized PMO materials. Computational tools were used to understand the interaction between CO_2 and CH_4 molecules and the different functionalities in the prepared PMOs. As referred above, the structure used to model the Ph-PMO material was functionalized in 33% of the phenylene moieties. In the case of the functionalization with the amino functional group, we have studied carefully the substitution of –H by $–NH_2$ in several different positions of the aromatic rings but only the two most favorable positions are shown in Figure 8.

-R group	A	B
$-NH_2$	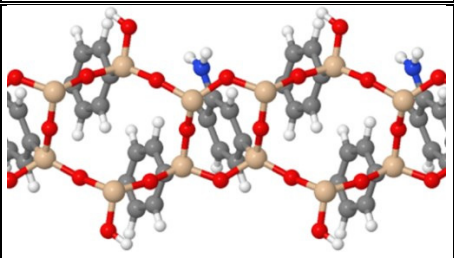	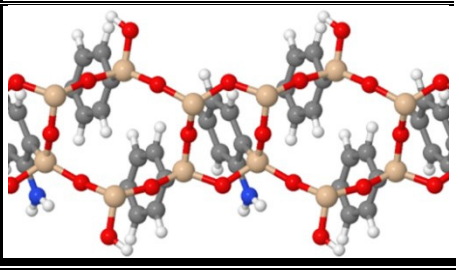

Figure 8. Side views of the two most favorable configurations for NH_2-Ph-PMOs. Color code for atomic spheres: N, blue and remaining atoms as in Figure 1.

The APTMS ($–Si(OH)_2C_3H_5NH_2$) group was grafted onto the free silanols (Si-OH) of the most favorable structures optimized for Ph-PMO and NH_2-Ph-PMO to obtain models of the

walls of the APTMS@Ph-PMO and APTMS@NH_2-Ph-PMO materials, respectively. Several different starting configurations of the APTMS moiety were considered because of the high number of degrees of freedom of this group. The two most favorable positions for each APTMS functionalized Ph-PMO are presented in Figure 9.

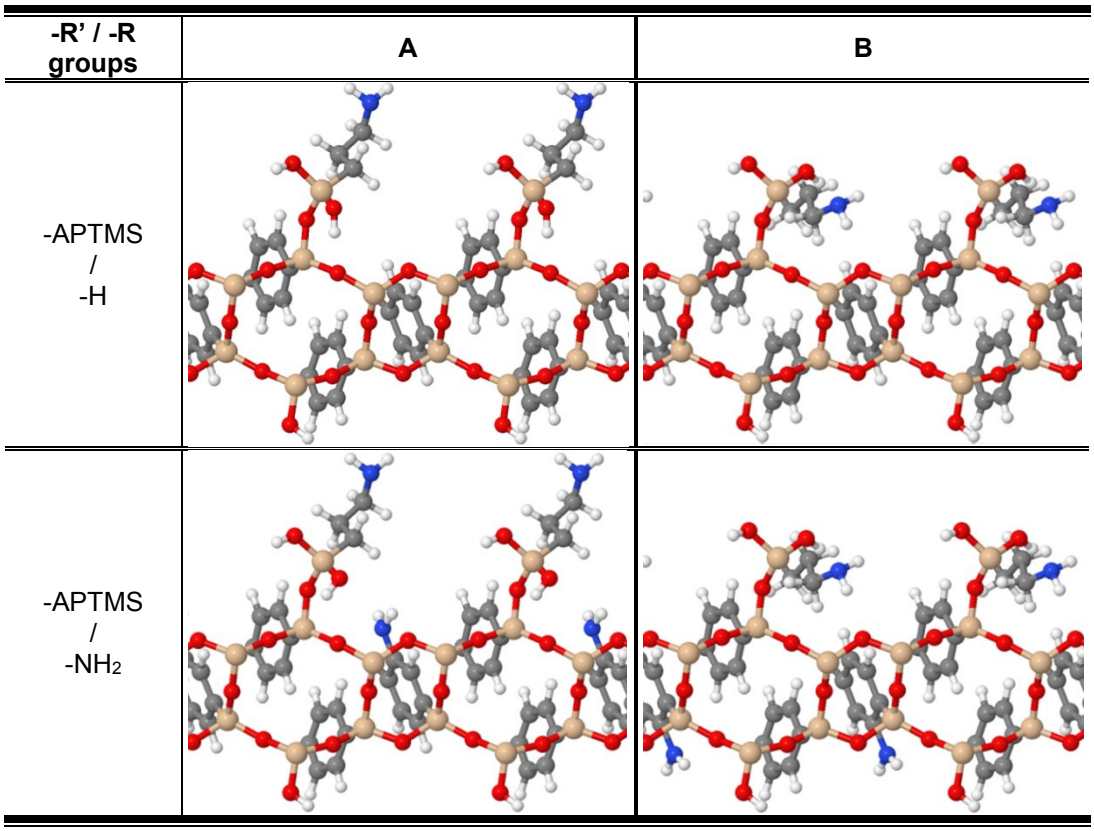

Figure 9. Side views of the two most favorable configurations optimized for APTMS@Ph-PMO (top) and APTMS@NH_2-Ph-PMO (bottom). Color code for atomic spheres as in Figure 8.

The adsorption energies for the CO_2 and CH_4 molecules interacting with each of the PMO models described above are reported in Table 2, and views of the most favorable locations are given in Figure 10. The PBE-D2 energies for CO_2 adsorption vary between -19.8 kJ·mol^{-1} in the case of the parent Ph-PMO and -29.0 kJ·mol^{-1} for the APTMS@Ph-PMO material, while for CH_4 the interaction energies are in the interval between -9.5 and -13.7 kJ·mol^{-1} for APTMS@NH_2-Ph-PMO and APTMS@Ph-PMO,

respectively. Thus, the interaction energies of CO_2 with the different materials are much higher than the interaction energies obtained for CH_4 and, despite the limitations associated to the structural models used and the non-consideration of kinetic data, the calculated results are in line with the strength of the Henry's constants calculated from experimental adsorption isotherms (Table 1). In particular, the interaction energies for CO_2 increase in the order Ph-PMO < NH_2-Ph-PMO < APTMS@NH_2-Ph-PMO < APTMS@Ph-PMO, which is the same order obtained for the Henry's constants for the CO_2 gas. The ratio between the adsorption energies calculated for CO_2 and CH_4 molecules on the same material shows the highest value for APTMS@NH_2-Ph-PMO and a decrease in the order APTMS@NH_2-Ph-PMO > NH_2-Ph-PMO > APTMS@Ph-PMO > Ph-PMO.

From the views of the optimized configurations shown in Figure 10 and from the values of selected atomic distances reported in Table S5 (SI) we conclude that CO_2 interacts preferentially with the silanol group in the case of Ph-PMO, with a SiOH···OCO nearest-neighbor distance of 2.28 Å. In the case of NH_2-Ph-PMO, the CO_2 interaction occurs with both the silanol and amino groups at nearest-neighbor distances of 2.45 and 2.60 Å, respectively. For APTMS@Ph-PMO, CO_2 interacts with both the amino group and an acidic hydrogen (**H20)** of the alkyl chain of the APTMS group at nearest-neighbor distances of 2.58 and 2.75 Å, respectively. The CO_2 in APTMS@NH_2-Ph-PMO interacts with the silanol group and an acidic hydrogen (**H20)** of the alkyl chain of the APTMS group, at nearest-neighbor distances of 2.45 and 2.62 Å, respectively. A direct relationship between geometric parameters and calculated adsorption energies is unclear, with the exception that in the case of the parent compound the CO_2 molecule is interacting with a single site on the PMO wall while in the aminated materials the most favorable interactions involve two sites. This is

likely to be the main cause for the significantly more favorable interaction energies observed in all the aminated materials with respect to the pristine Ph-PMO (Table 2).

Table 2. Calculated low-coverage adsorption enthalpies of CO_2 and CH_4 species in the four different aminated Ph-PMOs.

-R'/ -R groups	CO_2 Interaction Energy (kJ·mol^{-1})	CH_4 Interaction Energy (kJ·mol^{-1})	Ratio CO_2/CH_4
-H / -H	-19.8	-12.9	1.53
-H / -NH_2 (A)	-26.2	-11.7	2.24
-APTMS / -H (A)	-29.0	-13.7	2.12
-APTMS / -NH_2(A)	-25.9	-9.5	2.73

In the case of methane, the interactions seem to be predominantly with a hydrogen atom from the aromatic ring in the case of the Ph-PMO material; with the amino group in the case of NH_2-Ph-PMO; in the cavity defined by the hydrogen atoms from the silanol (**H29**) and amino (**H28**) groups and from the alkyl chain of the APTMS (**H20**) group in the case of APTMS@Ph-PMO; and with the hydrogen atom (**H29**) of one free silanol of the aminopropil group (APTMS) in the case of APTMS@NH_2-Ph-PMO. The nearest-neighbor distances (Table S5, SI) are 3.07, 2.36, 2.58 and 2.14 Å, respectively.

As in the case of CO_2, a direct relationship between the calculated energies and the selected geometrical parameters is not evident. Nevertheless, it arises that the interaction of methane with the models having an amino group in the aromatic ring is weaker than those calculated for the corresponding materials without such groups (cf. compare adsorption energies reported in Table 2 for Ph-PMO and APTMS@Ph-PMO with those for NH_2-Ph-PMO and APTMS@NH_2-Ph-PMO).

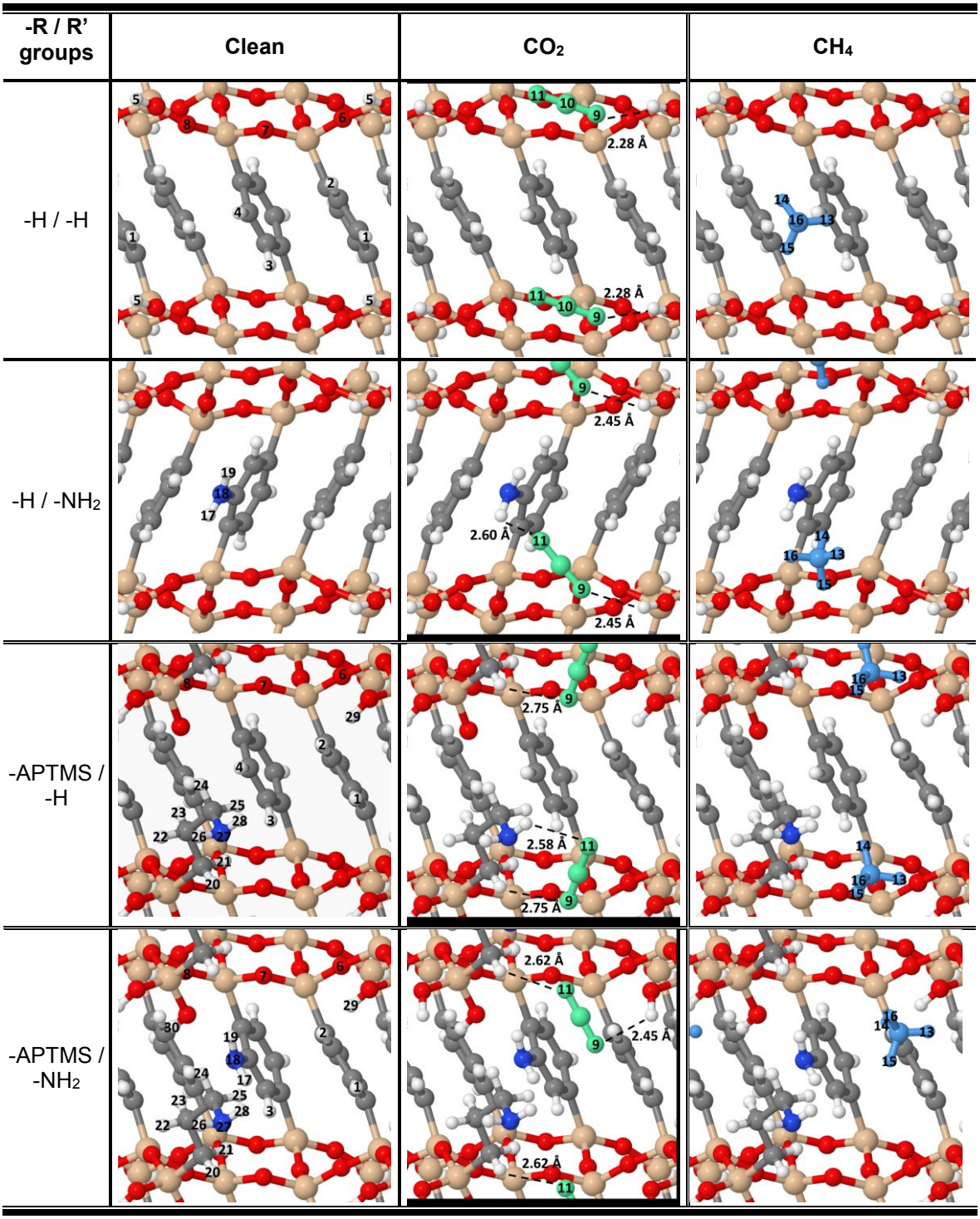

Figure 10. Top views of the optimized clean, and CO_2 or CH_4 covered aminated Ph-PMO materials. Color code for adsorbent atoms as in Figure 8, and light green and light blue are used for atoms in CO_2 and CH_4 adsorbates, respectively. The numbering is the same as used in Table S5 containing selected geometrical parameters.

From the pure CO_2 and CH_4 experimental adsorption in the prepared PMO, it is possible to conclude that all these materials adsorb similar amounts of methane, in very small quantities, while the CO_2 adsorption is much higher. Therefore, it is more relevant to examine the CO_2 interaction energies calculated for the prepared materials than the interaction energies obtained for CH_4. The correlation between the interaction energies obtained for the CO_2 molecules and the Henry's constants for the CO_2 adsorption in each material are in good agreement, showing that despite the inherent limitations of the computational model (for example, consideration of a single lowest energy adsorption site, thus neglecting entropic factors), it can be used to predict the potential of other functionalized phenylene-PMOs for the adsorption of CO_2 or for the separation of CO_2 from CH_4.

3.4. Molecular simulation of other R functionalized Ph-PMO materials. Since the interaction energies calculated with DFT for CO_2 and CH_4 in the parent and aminated Ph-PMOs compared well with the experimentally determined gas adsorption capacities of such materials, further DFT calculations were performed to understand how other functional groups (e.g. $–NO_2$, –NH-*i*-Pr, $–CH_2NH_2$ and $–SO_3H$) interact with CO_2 and CH_4, with the purpose of optimizing resources and avoiding the synthesis of ineffective materials. These functional groups were chosen on the basis of their different polarities and of the ease of preparation of PMO-functionalized materials.[17,18,21] To enable direct comparison with the results presented in the previous section, only one third of the aromatic phenylene moieties were functionalized with such groups. The two most favorable configurations for each new PMO derived from Ph-PMO obtained after full optimization are presented in Figure 11.

The interaction of CO_2 and CH_4 molecules with the two configurations in Figure 11 for each R-Ph-PMO was analyzed by DFT. The calculated interaction energies are reported in Table

3 and the final configurations for the two adsorbates interacting with each material are depicted in Figure 12. Selected geometrical parameters are supplied in Table S6 (SI).

The comparison of the energetic data in Tables 2 and 3 shows that the introduction of the nitro group (–NO_2) in the phenylene moieties of the Ph-PMOs increases slightly the interaction of both CO_2 (-2.1 kJ·mol^{-1}) and CH_4 (-0.4 kJ·mol^{-1}). These tiny differences seem to be associated to the interaction of the carbon atom of CO_2 and one of the hydrogen atoms of CH_4 with an oxygen atom of the nitro group (Table S6, SI). The DFT results suggest that nitrated materials are less promising than the aminated PMOs for this separation.

The introduction of an *iso*-propylamine group in the phenylene bridge of Ph-PMO leads to significant increases in the interaction energies calculated for both CO_2 (-7.8 kJ·mol^{-1}) and CH_4 (-4.7 kJ·mol^{-1}) when compared with the parent Ph-PMO value. However, relative to NH_2-Ph-PMO, the CO_2 energy is only slightly increased, while that of methane increases more significantly. These changes are most likely a consequence of improved interactions of CO_2 with the amine moiety and of methane with the propyl groups. Indeed, some authors [44,45] reported that propyl amines can improve the interaction with CO_2. Nevertheless, based on the DFT interaction energies calculated in this work, the NH-*i*-Pr-Ph-PMO material is anticipated to present similar CO_2 adsorption capacity but poorer selectivity for CO_2/CH_4 separations than those observed for NH_2-Ph-PMO. Since an additional synthetic step is required to obtain NH-*i*-Pr-Ph-PMO, the latter becomes less interesting than NH_2-Ph-PMO for this adsorption application.

Table 3. Calculated low-coverage interaction energies of CO_2 and CH_4 molecules in different **R** functionalized Ph-PMOs.

-R group	CO_2 Interaction Energy / kJ.mol^{-1}	CH_4 Interaction Energy / kJ.mol^{-1}	Ratio CO_2/CH_4
–**NO_2**	-21.9	-13.3	1.64
–**NH-*i*-Pr**	-27.6	-17.6	1.35
–**CH_2NH_2**	-31.1	-15.2	2.05
–**SO_3H**	-26.9	-10.6	2.54

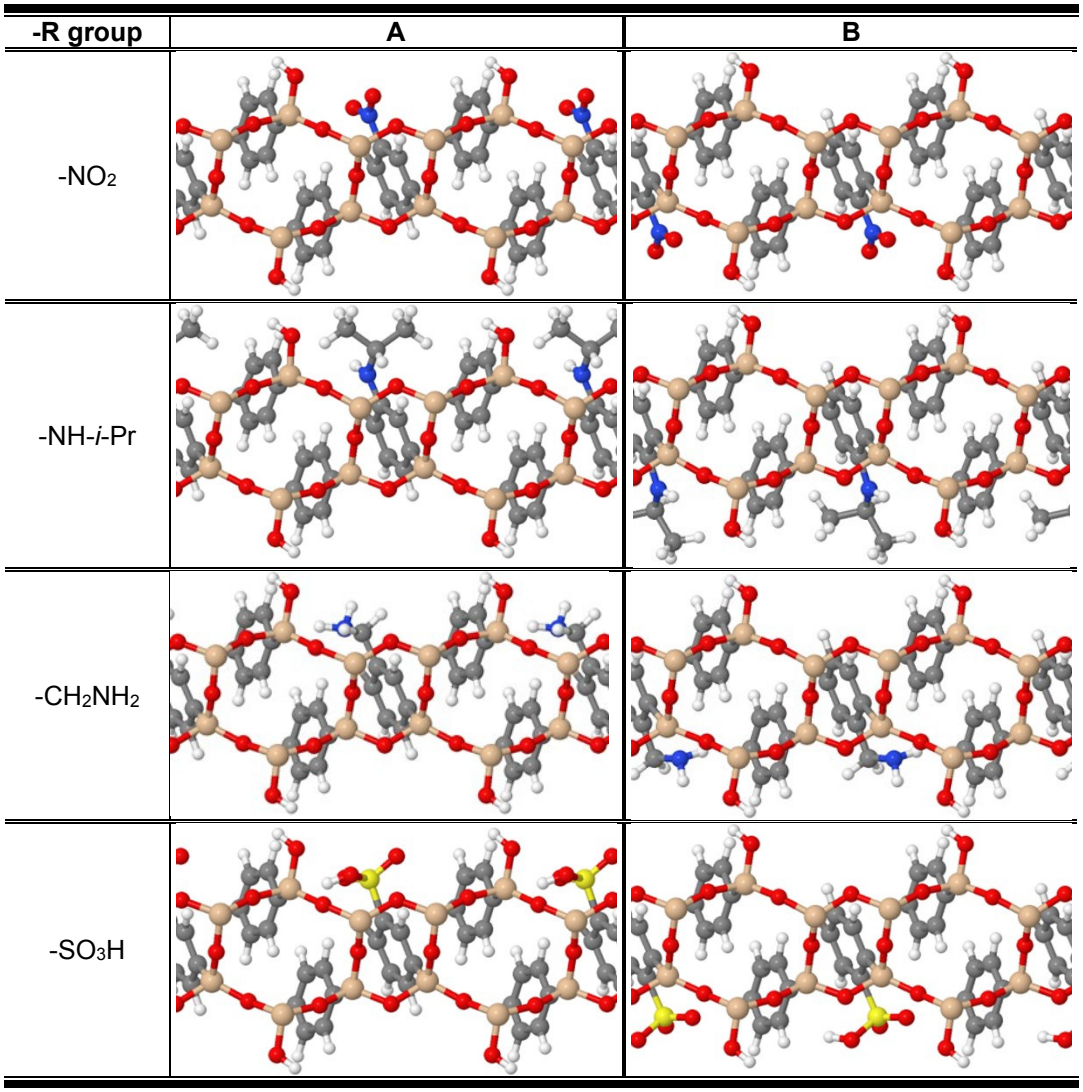

Figure 11. Side views of the two most favorable configurations for **R** functionalized Ph-PMOs.

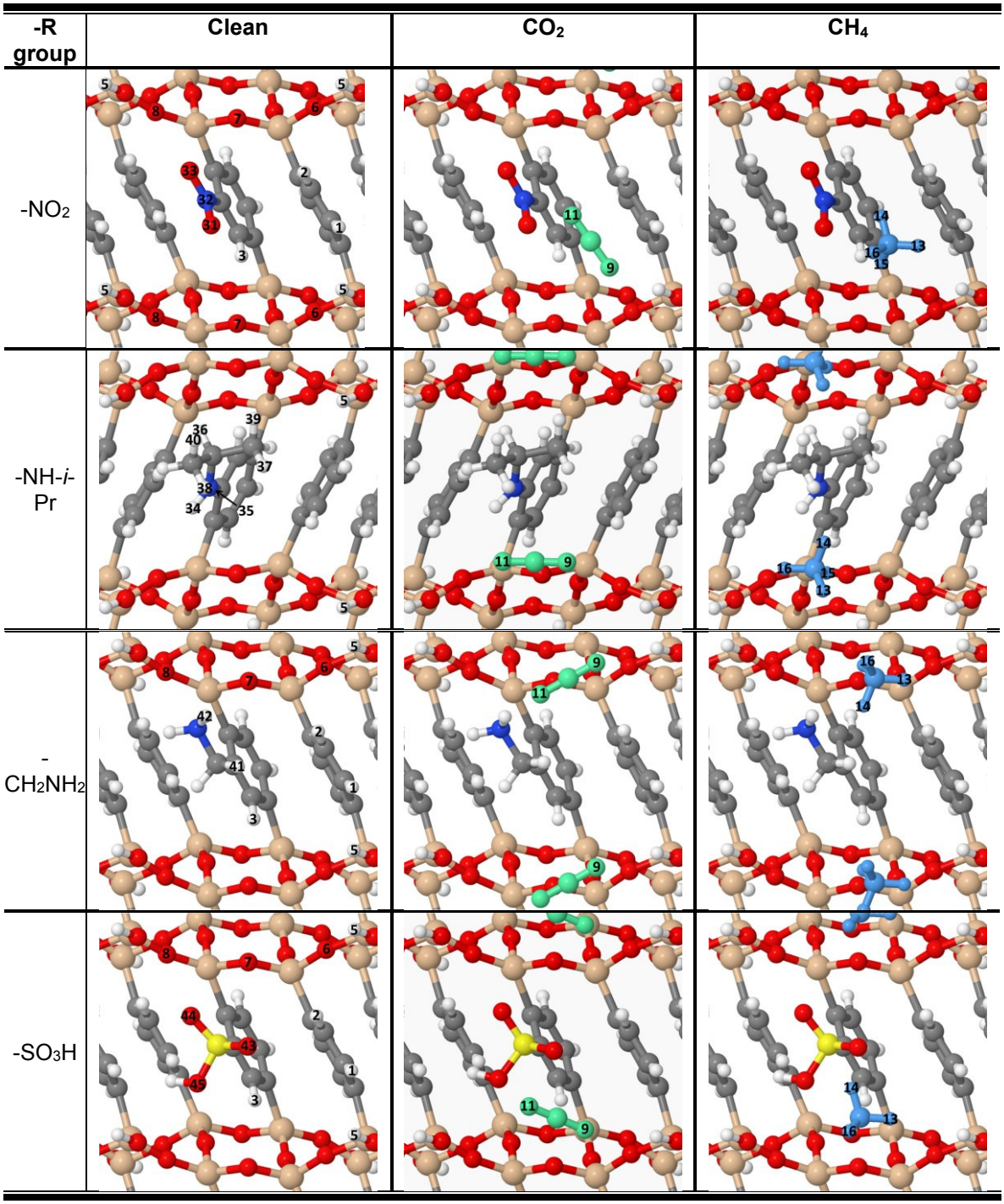

Figure 12. Top views of the most stable configurations for clean and CO_2 or CH_4 covered **R**-Ph-PMOs optimized at the PBE-D2 level of theory. The numbering is the same as used in Table S6 containing selected geometrical parameters.

The material with the $–CH_2NH_2$ functional group shows the strongest interaction energy with the CO_2 molecule of all Ph-PMOs studied in this work. The interaction energy is -31.1 $kJ{\cdot}mol^{-1}$, i.e., an increase of -2.1 kJ·mol when compared with APTMS@Ph-PMO, suggesting that the former material may show more interesting CO_2 adsorption affinity than the latter without significantly changing the selectivity of the CO_2/CH_4 separation.

Finally, the calculated energies for the substitution of a hydrogen atom in the phenylene ring by a sulfonic acid group ($–SO_3H$) suggest that the resulting material will have adsorption profiles for CO_2 and CH_4 similar to those displayed by NH_2-Ph-PMO and APTMS@NH_2-Ph-PMO. Interestingly, the CO_2 molecule interacts with the hydrogen atom from the -SiOH group but not with that from the $–SO_3H$ group. This suggests that the interaction with the former is more important and that the quite short distance between the –SiOH and the $-SO_3H$ groups hinders the formation of simultaneous contacts with these two groups.

4. CONCLUSIONS

Ph-PMOs functionalized with different types of amines were successfully prepared and characterized. The pristine and amine-functionalized Ph-PMO materials exhibit both meso- and molecular-scale orders observed by PXRD. These materials were tested for adsorption of pure CO_2 and CH_4 at 25 and 35 °C. All prepared materials presented much higher CO_2 adsorption than that of CH_4. The introduction of amines into the Ph-PMO material generally gave rise to an increase in the quantity of adsorbed CO_2 over the studied pressure range. More importantly, it significantly increased the Henry's constants of CO_2, growing in the order Ph-PMO < NH_2-Ph-PMO < APTMS@NH_2-Ph-PMO < APTMS@Ph-PMO, i.e., the

APTMS@Ph-PMO material has more affinity for CO_2 than any other PMO material. Thus, it was observed that the type of amine presents a dominant effect on the CO_2 sorption affinity, more so than the nitrogen content in the PMO channels, demonstrating that alkyl amines interact more favorably with CO_2 than aromatic amines. Furthermore, the observed reduction in surface area and pore volume upon functionalization is more than compensated by the increased affinity under the conditions studied here. After the adsorption study, the chemical integrity of the amine modified PMOs was evaluated by ^{13}C CP-MAS and ^{15}N CP-MAS NMR, indicating that PMO materials release the CO_2 after activation and can be reused.

Periodic DFT calculations were successfully used for the first time to evaluate the behavior of different kinds of amine-functionalized Ph-PMO on the CO_2 and CH_4 adsorption and correlated with the Henry's constants. The same trend was found in both DFT calculations and gas adsorption measurements, showing that this type of theoretical studies can be used to predict if a chemical modification of the PMO promotes an increase in the selectivity of CO_2 relative to CH_4. Furthermore, DFT calculation were also used to studied the preferential adsorption sites and interaction energies of CO_2 and CH_4 molecules on PMOs functionalized in the phenylene moieties with different groups ($–NO_2$, –NH-*i*-Pr, $–CH_2NH_2$, and $–SO_3H$), in order to guide the synthesis of new promising materials. It was found that the Ph-PMO functionalized with CH_2NH_2 is most likely to enhance CO_2 adsorption without changing significantly the adsorption of CH_4, and is thus a promising candidate for future experimental studies.

ASSOCIATED CONTENT

Supporting information (SI) available. Materials' characterization details and further data from PXRD, -196 °C N_2-sorption isotherms, ^{13}C, ^{29}Si and ^{15}N solid-state NMR, FTIR, TGA and EA experiments. Additional CO_2 and CH_4 experimental adsorption isotherms and selected computational structural data. This material is available free of charge via the Internet at http://pubs.acs.org.

AUTHOR INFORMATION

Corresponding Author

*José R. B. Gomes. E-mail: jrgomes@ua.pt. Fax: +351 234401470.

AUTHOR CONTRIBUTIONS

The manuscript was written through contributions of all authors. All authors have given approval to the final version of the manuscript.

FUNDING SOURCES

Fundação para a Ciência e a Tecnologia (FCT) and Fundo Europeu de Desenvolvimento Regional (FEDER): POCI-01-0145-FEDER-007679; UID/CTM/50011/2013; UID/MULTI/00612/2013; PTDC/EQU-EQU/099423/2008; FCOMP-01-0124-FEDER-010345; REDE/1509/RME/2005

NOTES

Any additional relevant notes should be placed here.

ACKNOWLEDGEMENTS

This work was developed in the scope of the projects POCI-01-0145-FEDER-007679 | UID/CTM/50011/2013 (CICECO), UID/MULTI/00612/2013 (CCB), UID/ECI/04028/2013 (CERENA), NORTE-07-0124-FEDER-000011 | UID/EQU/500230/2013 (LSRE), PTDC/EQU-EQU/099423/2008 (FCOMP-01-0124-FEDER-010345), financed by national funds through the FCT/MEC and co-financed by FEDER under the PT2020 Partnership Agreement. The authors are also grateful to FCT Programmes Ciência 2007 and Investigador FCT, to the Portuguese NMR Network (RNRMN), and to the National Network of electron microscopy and University of Aveiro: Project REDE/1509/RME/2005. The PhD grant SFRH/BD/80883/2011 (to M.A.O.L.) and the postdoc grant SFRH/BPD/65978/2009 (to M.S.) are also ackownledged.

Umberto Martinez and Gianfranco Pacchioni are acknowledged for kindly providing the structure of *p*-phenylenesilica corresponding to a sequence of six and four member rings with T^3 to T^2 ratio 2:1. The authors are also indebted to João Santos for fruitful discussions.

ABBREVIATIONS

APTMS, aminopropyltriethoxysilane; BTEB, 1,4-bis(triethoxysilyl)benzene; C_{12}TMA, dodecyltrimethylammonium bromide; CP, cross-polarization; DFT, density functional theory; EA, elemental analysis; FTIR, Fourier transform infrared; GGA, generalized-gradient approximation; MAS, magic-angle spinning; NMR, nuclear magnetic resonance; PAW, projector-augmented wave; PBE, Perdew-Burke-Ernzerhof; PMO, periodic mesoporous organosilica; Ph-PMO, periodic mesoporous phenylene-silica; PXRD, powder X-ray diffraction; SI, supporting information; TEM, transmission electron microscopy; TGA, thermogravimetric analysis.

REFERENCES

(1) Jaramillo, P.; Matthews, H. S. Landfill-Gas-to-Energy Projects: Analysis of Net Private and Social Benefits. *Environ. Sci. Technol.* **2005**, *39*, 7365–7373.

(2) Knaebel, K. S.; Reinhold, H. E. Landfill Gas: From Rubbish to Resource. *Adsorption* **2003**, *9*, 87–94.

(3) Lohila, A.; Laurila, T.; Tuovinen, J. P.; Aurela, M.; Hatakka, J.; Thum, T.; Pihlatie, M.; Rinne, J.; Vesala, T. Micrometeorological Measurements of Methane and Carbon Dioxide Fluxes at a Municipal Landfill. *Environ. Sci. Technol.* **2007**, *41*, 2717–2722.

(4) Rodrigues, A. E.; Grande, C. A. Biogas to Fuel by Vacuum Pressure Swing Adsorption I. Behavior of Equilibrium and Kinetic-Based Adsorbents. *Ind. Eng. Chem. Res.* **2007**, *46*, 4595–4605.

(5) Yin, C. Y.; Aroua, M. K.; Daud, W. M. A. W. Review of Modification of Activated Carbon for Enhancing Contaminant Uptakes from Aqueous Solutions. *Sep. Purif. Technol.* **2007**, *52*, 403–415.

(6) Delahay, G.; Coq, B. Pollution Abatement Using Zeolites: State of the Art and Further Needs. *Catal Sci. Ser.* **2002**, *3*, 345–374.

(7) Bhattacharyya, K. G.; Gupta, S. Sen. Adsorption of a Few Heavy Metals on Natural and Modified Kaolinite and Montmorillonite: A Review. *Adv. Colloid Interface Sci.* **2008**, *140*, 114–131.

(8) Gadd, G. M. Biosorption: Critical Review of Scientific Rationale, Environmental Importance and Significance for Pollution Treatment. *J. Chem. Technol. Biotechnol.* **2009**, *84*, 13–28.

(9) Lin, S. H.; Juang, R.-S. Adsorption of Phenol and Its Derivatives from Water Using Synthetic Resins and Low-Cost Natural Adsorbents: A Review. *J. Environ. Manage.* **2009**, *90*, 1336–1349.

(10) Pan, B.; Zhang, W.; Lv, L.; Zhang, Q.; Zheng, S. Development of Polymeric and Polymer-Based Hybrid Adsorbents for Pollutants Removal from Waters. *Chem. Eng. J.* **2009**, *151*, 19–29.

(11) Jal, P. K.; Patel, S.; Mishra, B. K. Chemical Modification of Silica Surface by Immobilization of Functional Groups for Extractive Concentration of Metal Ions. *Talanta* **2004**, *62*, 1005–1028.

(12) Walcarius, A.; Mercier, L. Mesoporous Organosilica Adsorbents: Nanoengineered Materials for Removal of Organic and Inorganic Pollutants. *J. Mater. Chem.* **2010**, *20*, 4478–4511.

(13) Asefa, T.; MacLachlan, M. J.; Coombs, N.; Ozin, G. A. Periodic Mesoporous Organosilicas with Organic Groups inside the Channel Walls. *Nature* **1999**, *402*, 867–871.

(14) Inagaki, S.; Guan, S.; Fukushima, Y.; Ohsuna, T. Novel Mesoporous Materials with a Uniform Distribution of Organic Groups and Inorganic Oxide in Their Frameworks. *J. Am. Chem. Soc.* **1999**, *121*, 9611–9614.

(15) Melde, B. J.; Holland, B. T.; Blanford, C. F.; Stein, A. Mesoporous Sieves with Unified Hybrid Inorganic/Organic Frameworks. *Chem. Mater.* **1999**, *11*, 3302–3308.

(16) Lourenço, M. A. O.; Siquet, C.; Santos, J. C.; Jorge, M.; Gomes, J. R. B.; Ferreira, P. Understanding the Performance of Pristine and Aromatic Amine-Modified Periodic Mesoporous Phenylene-Silicas for CO_2 and CH_4 Adsorption. *Submitted.*

(17) Ohashi, M.; Kapoor, M. P.; Inagaki, S. Chemical Modification of Crystal-like Mesoporous Phenylene-Silica with Amino Group. *Chem. Commun.* **2008**, *7*, 841–843.

(18) Lourenço, M. A. O.; Siegel, R.; Mafra, L.; Ferreira, P. Microwave Assisted N-Alkylation of Amine Functionalized Crystal-like Mesoporous Phenylene-Silica. *Dalt. Trans.* **2013**, *42*, 5631–5634.

(19) Sim, K.; Lee, N.; Kim, J.; Cho, E.-B.; Gunathilake, C.; Jaroniec, M. CO2 Adsorption on Amine-Functionalized Periodic Mesoporous Benzenesilicas. *ACS Appl. Mater. Interfaces* **2015**, *7*, 6792–6802.

(20) Ferreira, P.; Bispo, C.; Lourenço, M. A. O.; Gomes, J. R. B.; Bion, N.; Vigier, K.; Jérôme, F. Making Periodic Mesoporous Organosilicas Functional Materials. In *Comprehensive Guide for Mesoporous Materials, Volume 4: Application and Commercialization*; Aliofkhazraei, M., Ed.; 2015; pp 261–295.

(21) Inagaki, S.; Guan, S.; Ohsuna, T.; Terasaki, O. An Ordered Mesoporous Organosilica Hybrid Material with a Crystal-like Wall Structure. *Nature* **2002**, *416*, 304–307.

(22) Bion, N.; Ferreira, P.; Valente, A.; Gonçalves, I. S.; Rocha, J. Ordered Benzene-Silica Hybrids with Molecular-Scale Periodicity in the Walls and Different Mesopore Sizes. *J. Mater. Chem.* **2003**, *13*, 1910–1913.

(23) Corriu, R. J. P.; Moreau, J. J. E.; Thepot, P.; Man, M. W. C. New Mixed Organic-Inorganic Polymers: Hydrolysis and Polycondensation of Bis(trimethoxysilyl)organometallic Precursors. *Chem. Mater.* **1992**, *4*, 1217–1224.

(24) Myers, A. L. Equation of State for Adsorption of Gases and Their Mixtures in Porous Materials. *Adsorption* **2003**, *9*, 9–16.

(25) Pires, J.; Saini, V. K.; Pinto, M. L. Studies on Selective Adsorption of Biogas Components on Pillared Clays: Approach for Biogas Improvement. *Environ. Sci. Technol.* **2008**, *42*, 8727–8732.

(26) Jorge, M.; Fischer, M.; Gomes, J. R. B.; Siquet, C.; Santos, J. C.; Rodrigues, A. E. Accurate Model for Predicting Adsorption of Olefins and Paraffins on MOFs with Open Metal Sites. *Ind. Eng. Chem. Res.* **2014**, *53*, 15475–15487.

(27) Kresse, G.; Hafner, J. Ab Initio Molecular Dynamics for Liquid Metals. *Phys. Rev. B* **1993**, *47*, 558–561.

(28) Kresse, G.; Furthmüller, J. Efficiency of Ab-Initio Total Energy Calculations for Metals and Semiconductors Using a Plane-Wave Basis Set. *Comput. Mater. Sci.* **1996**, *6*, 15–50.

(29) Kresse, G.; Furthmüller, J. Efficient Iterative Schemes for Ab Initio Total-Energy Calculations Using a Plane-Wave Basis Set. *Phys. Rev. B* **1996**, *54*, 11169–11186.

(30) Perdew, J. P.; Burke, K.; Ernzerhof, M. Generalized Gradient Approximation Made

Simple. *Phys. Rev. Lett.* **1996**, *77*, 3865–3868.

(31) Grimme, S. Semiempirical GGA-Type Density Functional Constructed with a Long-Range Dispersion Correction. *J. Comput. Chem.* **2006**, *27*, 1787–1799.

(32) Ramalho, J. P. P.; Gomes, J. R. B.; Illas, F. Accounting for van Der Waals Interactions between Adsorbates and Surfaces in Density Functional Theory Based Calculations: Selected Examples. *RSC Adv.* **2013**, *3*, 13085–13100.

(33) Fajín, J. L. C.; Cordeiro, M. N. D. S.; Gomes, J. R. B.; Illas, F. On the Need for Spin Polarization in Heterogeneously Catalyzed Reactions on Nonmagnetic Metallic Surfaces. *J. Chem. Theory Comput.* **2012**, *8*, 1737–1743.

(34) Martinez, U.; Pacchioni, G. Interaction of CO, CO_2 and CH_4 with Mesoporous Organosilica: Periodic DFT Calculations with Dispersion Corrections. *Microporous Mesoporous Mater.* **2010**, *129*, 62–67.

(35) Camarota, B.; Ugliengo, P.; Garrone, E.; Arean, C. O.; Delgado, M. R.; Inagaki, S.; Onida, B. IR and Computational Characterization of CO Adsorption on a Model Surface, the Phenylene Periodic Mesoporous Organosilca with Crystalline Walls. *J. Phys. Chem. C* **2008**, *112*, 19560–19567.

(36) Kresse, G.; Joubert, D. From Ultrasoft Pseudopotentials to the Projector Augmented-Wave Method. *Phys. Rev. B* **1999**, *59*, 1758–1775.

(37) Comotti, A.; Bracco, S.; Valsesia, P.; Ferretti, L.; Sozzani, P. 2D Multinuclear NMR, Hyperpolarized Xenon and Gas Storage in Organosilica Nanochannels with Crystalline Order in the Walls. *J. Am. Chem. Soc.* **2007**, *129*, 8566–8576.

(38) Sing, K. S. W.; Everett, D. H.; Haul, R. A. W.; Moscou, L.; Pierotti, R. A.; Rouquerol, J.; Siemieniewaska, T. Reporting Physisorption Data for Gas/solid Systems with Special Reference to the Determination of Surface Area and Porosity. *Pure Appl. Chem.* **1985**, *57*, 603–619.

(39) Beck, J. S.; Vartuli, J. C.; Roth, W. J.; Leonowicz, M. E.; Kresge, C. T.; Schmitt, K. D.; Chu, C. T. W.; Olson, D. H.; Sheppard, E. W. A New Family of Mesoporous Molecular Sieves Prepared with Liquid Crystal Templates. *J. Am. Chem. Soc.* **1992**, *114*, 10834–10843.

(40) Zwanzig, R. W. Influence of Molecular Electric Quadrupole Moments on Dielectric Constants. *J. Chem. Phys.* **1956**, *25*, 211–216.

(41) Myers, A. L.; Prausnitz, J. M. Thermodynamics of Mixed-Gas Adsorption. *AIChE J.* **1965**, *11*, 121–127.

(42) Pinto, M. L.; Pires, J.; Rocha, J. Porous Materials Prepared from Clays for the Upgrade of Landfill Gas. *J. Phys. Chem. C* **2008**, *112*, 14394–14402.

(43) Pinto, M. L.; Mafra, L.; Guil, J. M.; Pires, J.; Rocha, J. Adsorption and Activation of CO_2 by Amine-Modified Nanoporous Materials Studied by Solid-State NMR and $^{13}CO_2$ Adsorption. *Chem. Mater.* **2011**, *23*, 1387–1395.

(44) Xue, Q.; Liu, Y. Mixed-Amine Modified SBA-15 as Novel Adsorbent of CO_2 Separation for Biogas Upgrading. *Sep. Sci. Technol.* **2011**, *46*, 679–686.

(45) De Canck, E.; Ascoop, I.; Sayari, A.; Van Der Voort, P. Periodic Mesoporous

Organosilicas Functionalized with a Wide Variety of Amines for CO_2 Adsorption. *Phys. Chem. Chem. Phys.* **2013**, *15*, 9792–9799.

Table of Contents Graphic